VNU Journal of Science: Mathematics – Physics, Vol. 32, No. 3 (2016) 1-10

Theoretical Prediction of ZnO Nanoporous Allotropes with Triangular Hollow

Nguyen Thi Thao[1,2], Vu Ngoc Tuoc[1,*]

[1]*Institute of Engineering Physics, Hanoi University of Science and Technology, 1 Dai Co Viet, Hanoi, Vietnam*

[2]*Hong Duc University, 307 Le Lai, Thanh Hoa, Vietnam*

Received 05 September 2016
Revised 25 September 2016; Accepted 30 September 2016

Abstract: The advancement of technology has now made to enable not only growth materials in layer-by-layer or even in sub-layer with a desired ingredient. Further, it is expected to enable to manipulate on material layers at the desired address. This opens up opportunities for creating porous structures with specific allotropes - the purpose of materials engineering geometry. Zinc oxide (ZnO) material, along with wurtzite and zinblende, has been found in a large number of allotropes with substantially different properties, and hence, applications. Therefore, predicting and synthesizing new classes of ZnO allotropes is of great significance and has been gaining considerable interest. Herein, we perform a density functional theory based study, predicting several new series of ZnO hollow structures using the engineering geometry approach. The geometry of the building blocks allows for obtaining a variety of triangular, low-density nanoporous, and flexible hollow structures. We discuss their stability by means of the free energy computed within the lattice-dynamics approach. We show that all the reported structures are wide band gap semiconductors. Their electronic band structures are finally examined in detail.

Keywords: Nanoporous, Density Functional Theory (DFT), semiconductor.

1. Introduction

To date, inorganic *open-framework* (nanoporous) materials has quickly become an intense research area [1, 2]. Such the nanoporous materials are promising for sustainability applications, e.g. such as catalysis, gas separation, water purification, and batteries. Experimentally, the primary problem is to find the possessing channels that are capable to synthesize these nanoporous materials, e.g., those with base hollows/pores in the nanoscale. Theoretically, searching for new and interesting hollow allotropes is not only essential but also challenging [3]. Over the time, the number of structural types of unique nanoporous frameworks shown in the International Zeolite Association (IZA) database has been growing rapidly, from 27 in 1970, to 38 in 1978, 64 in 1988, 98 in 1996 and 174 in 2007 [4, 5].

Benefited from the most advances in self-assembly technology, nano- and micro-scale clusters can now be organized into a variety of the ordered three-dimensional (3D) lattices, opening up the

*Corresponding author. Tel.: 84- 989631799
Email: tuoc.vungoc@hust.edu.vn

possibility of designing nanoporous material structures from a set of atomic-level secondary building blocks [5-7]. Recently, Bauer *et al*. [8] reported that pyrolysis of polymeric microlattices have overcome the limitation of 3D lithography technologies and created ultra-strong glassy carbon nanolattices with diameters as small as 200 nm. The *strength-to-density* ratios of these low-density metamaterials with a honeycomb topology are close to the bulk diamond value.

The ZnO-based nanoporous materials are technologically promissing materiasl since ZnO is an important semiconductor, which can be easily realized in many different nanostructures, offering an excellent possibility for band gap and luminescent properties engineering, e.g. via core-shell or superlattice nano-heterostructures [9.10]. Further ZnO is piezoelectric material utilised in nanowire-based nanogenerators [11] whereas its room-temperature ferromagnetism induced by suitable dopants/defects (oxygen vacancies) found applications in spintronics [12, 13]. Due to the excellent bio-compatibility and optical and electronic properties, ZnO nanostructures are important ingredients of the new generations of optoelectronic devices [14, 15]. So far, realizing ZnO in new structures and/or allotropes is of considerable interest. Beside the traditional experimental approach, many *low-density* structures/allotropes of ZnO have been predicted computationally from first principles recently [15-20].

In the present paper, we propose a scheme for designing several series of hollow (porous) ZnO structures. Our approach relies on patterning triangular hollows onto the ZnO wurtzite bulk structure, keeping its chemical composition unchanged. We argue that this approach could provide a viable way to design nanoporous materials models computationally. We discuss the stability and the electronic structures of these materials based on calculations within the formalism of density functional based tight binding (DFTB).

2. Computational details

2.1. Theoretical structure prediction approach

In this section, following our recent approach for theoretically predicting ZnO crystal hollow structures [21], the secondary building blocks were chosen to be high in symmetries and large in HOMO-LUMO gap, which generally-believed criteria of stability [19, 20]. Via linking scheme of these secondary building blocks, many kinds of low-density framework ZnO materials with varying porosity have been proposed [4, 6, 8, 18, 20, 22]. Starting out from a bulk super cell of ZnO, we engrave out some pores with triangular pattern, leaving out the frame work of same hexagonal symmetry like wurtzite. The structure is subsequently be symmetrized and centerized to get the primitive cell. Then structures are energetically relaxed to get the final structure reported in characteristic Table.

The nanoporous allotropes reported herein are characterized by their wall and hollow size. The triangular hollow size – an equilateral triangle side, *n*, is measured in the unit of hexagonal block size (see Fig.1). The hollow wall is defined as the thickness between the hollows also is measured in number of hexagonal block layer, which can be single wall (SW), double wall (DW), triple wall (TW) and four wall (4W). Therefore, a structure labeled as SW-2 will have triangular hollows of size 2 which are spaced by single walls. For the illustration purpose, only the several smallest images for each series of structures are shown in Fig.1.

2.2. Density functional based tight binding plus method

Our calculations were performed within the spin-polarized, charge self-consistent, density functional based tight binding plus (DFTB+) approach [23-26]. This method is based on a second-

order expansion of the spin-dependent Kohn-Sham total energy functional with respect to a given reference charge and magnetization density. With all matrix elements and orbitals are derived from density functional calculations, DFTB method relies on a small basis set of atomic orbitals and two-center non-orthogonal Hamiltonian, allowing extensive use of look-up table. The Kohn-Sham equation is solved self-consistently using Mulliken charge projection. This approach has been proven to give transferable and accurate interaction potential as well as numerical efficiency allowing molecular dynamic simulation of supercell containing several hundreds to a thousand atoms. More details on DFTB+ can be found in Refs. [24, 25], and references therein. In our calculations the parameter and its transferability have been successfully applied in several previous DFTB works [27,28]. The benchmark for the DFTB+ numerical scheme used herein has been carried out in our recent study [21] using density functional theory (DFT) method as implemented in *Vienna Ab-initio simulation package* [29,30] for some ZnO hexagonal hollow structures with the Perdew-Burke-Ernzerhof (PBE) [31], PBEsol [32], and Heyd-Scuseria-Ernzerhof (HSE06) [33] functional. Comparison there shows the excellent agreement between DFT and DFTB+ results and claims that DFTB+ is a reasonable method for our work.

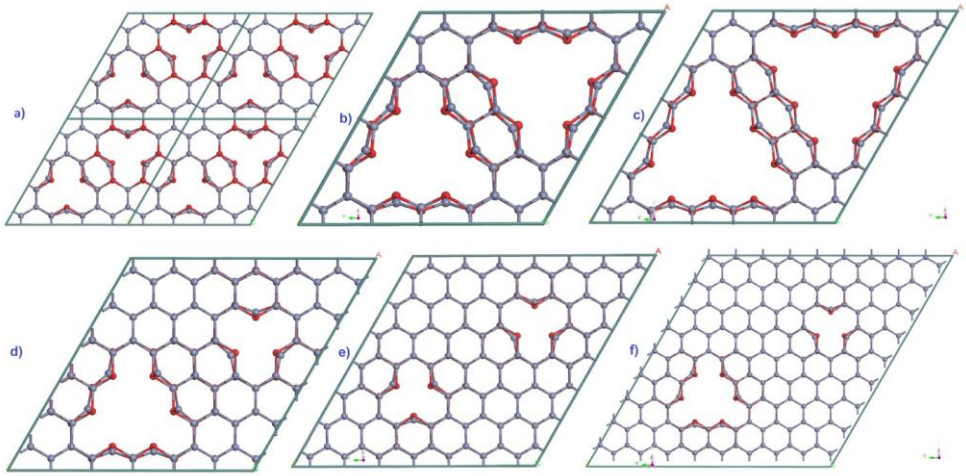

Figure 1. The ZnO nanoporous triangular hollow structures designed in this work (a) SW-2, (b) SW-3, (c) SW-4, (d) DW-2 (e) TW-2 (f) 4W-2. Small (red) balls are O atoms, big (gray) ones are Zn. The cyan rhombus frame is the unit cell.

3. Results and dicussions

3.1. Cohesive energy, phase stability and equation of state

To discuss the stability of the predicted nanoporous ZnO structures, we calculated the total binding energy per ZnO-pair vs volume and the bulk modulus by nonlinearly fitting obtained data to the Birch-Murnaghan equation of states (EOS), as performed in Ref. [34]. The results are presented in Fig. 2a in comparison with those of the wurtzite ZnO.

During the optimization process, all the designed hollow structures survive without structural collapse, indicating that they are physically relevant and might actually lead to low-density nanoporous phases of ZnO. As shown in Fig.2a, Table 1, structures with thicker wall are lower in binding energy. All of these structures are, however, higher than wurtzite ZnO in binding energy,

differing in internal-surface energy connected to the hollow size or porosity. The influence of such internal surface as well as the internal-surface-to-volume ratio can be examined by considering the *average* coordination number, which is generally below four, the characteristic value of wurtzite ZnO (see Table 1). The calculated bulk modulus (BM), see Fig.2b, Fig. 3a and Table 1, indicate that structures with thicker thickness are generally more stable than the lower one.

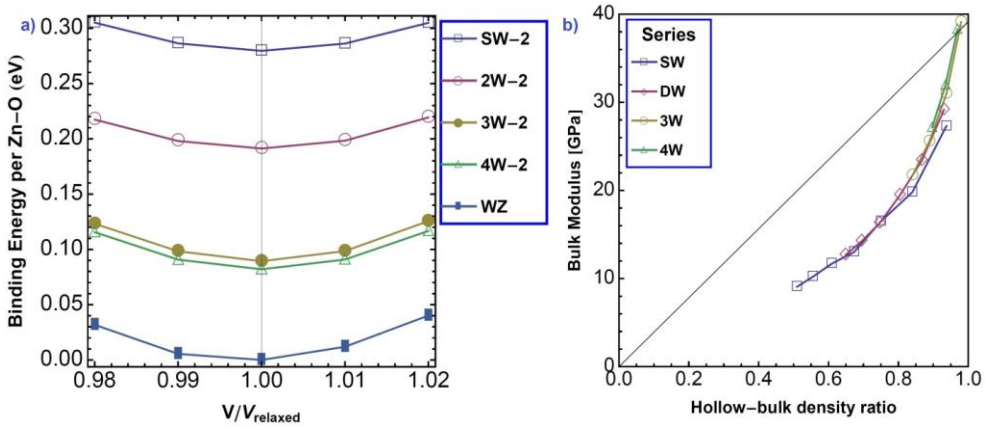

Figure 2. a) for ZnO-wutzite and all the smallest hollow size structures (n=2) of each series, total binding energy per Zn-O pair vs relative volume, i.e. curve for EOS fitting. b) Bulk modus obtained by using the third-order Birch−Murnaghan EOS, vs *hollow-to-bulk* density ratio.

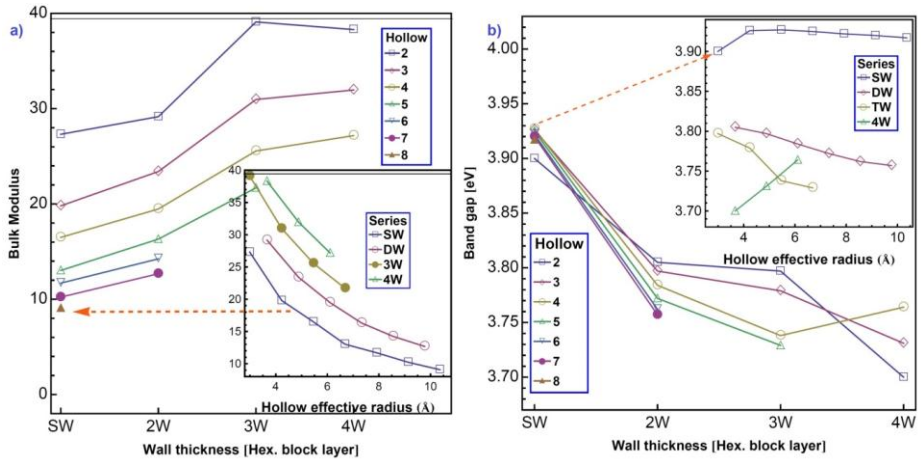

Figure 3. a) Bulk modulus vs. wall thickness and hollow size b) Band gap vs. wall thickness and hollow size of the studied series.

To discuss the structural stability at finite temperatures, we estimated the free energy of these crystals via the phonon bands structure [35], calculated by the MODES tool as implemented in DFTB+ [26]. This is presumably one of the most desirable finite-temperature quantities as it determines pretty much the essential characters of a crystal, e.g. among various possibilities, the structures with lowest-possible free energy are considered to be thermodynamically more stable. The dynamical stability of these hollow structures can also be accessed by their vibrational frequency spectra. Because there is no imaginary-frequency mode is found, the predicted structures are located at the real minimum of the

potential energy surface. Their phonon DOS are essentially similar, typically characterized by four prominent peaks in the lower frequency range of 100-250 cm^{-1} and three or four in the higher 450-600cm^{-1} region (see Fig. 4). Their free energies per atom as a function of temperatures from 0 to 500 K show the energy favorability orders toward the thicker wall as well as smaller hollow as expected.

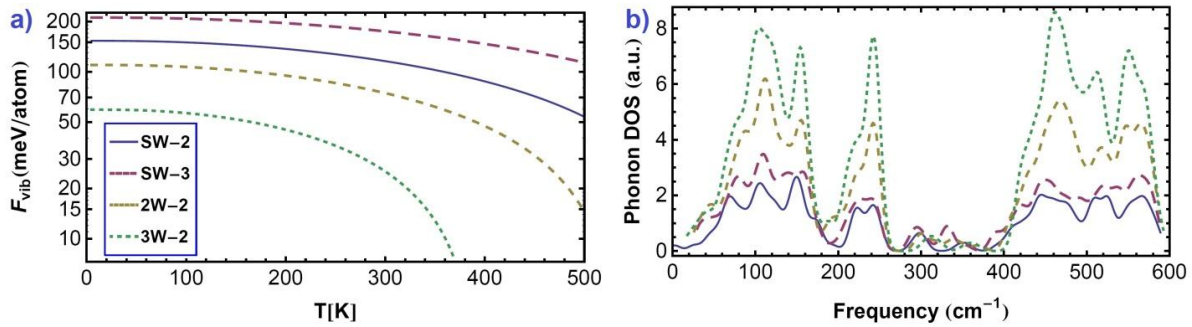

Figure 4. (a) Helmholtz free energies, referenced to the DFTB+ energy of 3W-2, of the considered structures and (b) phonon DOS of them.

3.2. Electronic band structure

To determine whether the ZnO nanoporous hollow phases, if synthesized, would possess novel properties, one should explore their electronic structures. Fig. 3b shows the band gap vs. their hollow size and wall thickness. It is noted that they all are below the wurtzite one. Our calculations show that the band gap varies from 3.7eV for 4W to 3.9eV for SW among the series. It is noted that within the used scheme, DFTB+ calculations overestimate the band gap, which is 3.44 eV for wurtzite ZnO from low temperature experimental measurements [20, 36]. We obtained the ZnO wurtzite band gap of 4.16eV, which agrees well with that reported in Ref. [27]. Moreover, our calculated ZnO zincblende band gap is 3.73eV, which can be considered close enough to the experimental value [36]. Interestingly, the results also show that all the new phases are still wide band gap semiconducting with direct gap at the Gamma point. Their band structures are similar to that of wurtzite ZnO only in the Gamma-A direction of the Brillouin zone, i.e. [001] direction. On the other hand, the designed hollows result in major differences in the cross section direction, causing the electronic band *flattening* (see Fig. 4). The reason for this observation, as pointed out by Sponza *et al*. [36], is due to the electrostatic potentials acting on anions V_O and cations V_{Zn} that results in a contribution $V = V_O - V_{Zn} > 0$ to the atomic level separation and to the gap width. Qualitatively, in denser local environments, V is larger. This trend is well obeyed in our studied hollow ZnO series while considering denser polymorphs, as seen in Fig. 3b. Further we also observed the week dependence of band gap on the hollow size and considerable dependence on the wall thickness which follow up the rule of quantum confinement as stated in [37] as decreasing the wall thickness increasing the band-gap energy. For smaller gap in the first structure of some series, e.g. SW-2 comparing to SW-3, the well-known phenomenon [37] ascribed to the in-gap surface states appearing inside the gap region. The dangling bonds at the internal surface causing surface relaxation which can be observed by the movement in-side of the anion (Zn) sites, results in the shrinkage of the wall's outer surface (Fig. 1). The role of internal surface effect become smaller with the thicker wall, e.g. 3W-2, 4W-2. It is agreed with Demiroglu *et al*. [17] that the regular void formation in a dense crystal removes atoms and thus their band-forming capacity, resulting in smaller bandwidths. This also is the reason of band gap flattening behavior, which increases with the increasing the hollow size (see Fig. 5), i.e. the internal hollow void space restricts

the overlap in cross-sectional direction throughout the crystal. It is the effect of porosity to reduce the band formation [38, 39], following the expected behavior in quantum confinement [37].

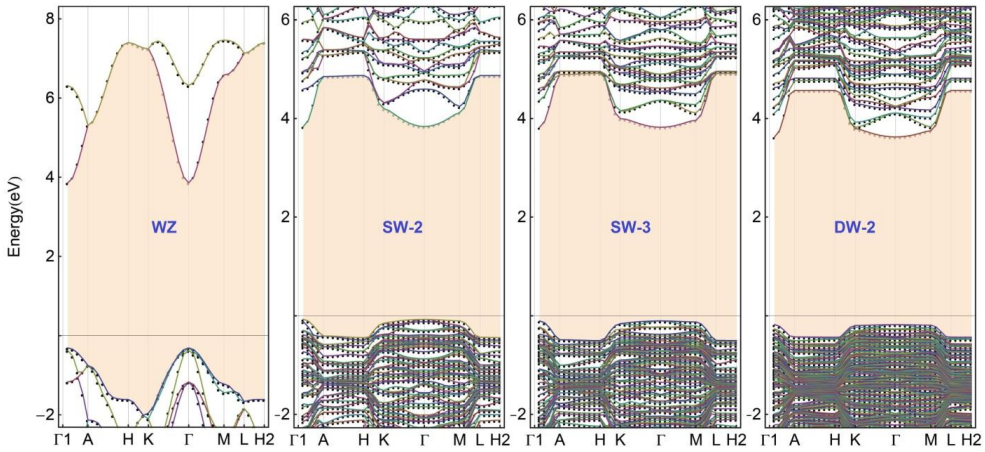

Figure 5. Band structure of ZnO wurtzite bulk, SW-2, SW-3, DW-2. Fermi energies are set to zero.

Table 1. Calculated characteristics of a representative of each series from studied structures.

Structures	**SW-2**	**SW-3**	**SW-4**	**SW-5**	**SW-6**	**SW-7**	**SW-8**	**DW-2**	**DW-3**	**DW-4**
Mass density (gcm^{-3})	4.965	4.424	3.983	3.530	3.189	2.903	2.663	4.954	4.665	4.264
Volume/at ($Å^3$/at)	13.610	15.276	17.158	19.146	21.192	25.275	25.374	13.640	14.675	15.88
Part. density ($10^{23}cm^{-3}$)	60.735	84.655	108.58	132.52	156.47	180.43	204.39	134.73	170.68	206.63
Coord. number	3.80	3.71	3.67	3.64	3.62	3.60	3.59	3.87	3.82	3.80
Crystal structure	Hex.	Hex.	Hex.	Hex.	Hex.	Hex.	Hex.	Hex.	Hex.	Hex.
Symmetry groups	$P6_3/mc$ IT 186	$P6_3/mc$ IT 186	$P6_3/mc$ IT 186	$P6_3/mc$ IT 186	$P6_3/mc$ IT 186	$P6_3/mc$ IT 186	$P6_3/mc$ IT 186	$P3_1m$ IT 156	$P3_1m$ IT 156	$P3_1m$ IT 156
Unit cell (atoms)	60	84	108	132	156	180	204	134	170	206
Lat. param. Å (a,c)	13.142 5.418	16.512 5.435	19.828 5.442	23.146 5.447	26.466 5.450	29.785 5.453	33.103 5.454	19.765 5.403	23.074 5.411	26.383 5.416
Average bond Å	2.005	2.001	1.999	1.997	1.996	1.995	1.995	2.009	2.007	2.006
Average angle Zn-O-Zn/O-Zn-O	109.18 110.46	109.00 110.98	108.89 111.30	108.81 111.80	108.76 111.65	108.72 111.76	108.69 111.85	109.18 110.11	109.07 110.33	109.00 110.48
Band gap eV	3.500	3.926	3.927	3.925	3.922	3.920	3.917	3.885	3.797	3.784
UC Connolly surface area $Å^2$	86.25	220.37	342.24	466.26	592.33	716.38	842.34	148.87	274.92	399.36

UC Pore vol. Å^3	49.78	238.33	517.92	909.15	1392.2	2003.1	2694.9	132,57	367.01	691.74
Num vib.mod.	180	252	324	396	468	540	612	402	510	618
Bulk modulus	27.31	19.8	16.40	13.02	11.69	10.22	9.07	29.16	23.40	19.47

Structures	**DW-5**	**DW-6**	**DW-7**	**TW-2**	**TW-3**	**TW-4**	**TW-5**	**4W-2**	**4W-3**	**4W-4**
Mass density (gcm^{-3})	3.952	3.672	3.424	5.240	5.004	4.741	4.474	5.815	4.995	4.785
Volume/at (Å^3/at)	17.101	18.402	19.936	2.895	13.504	14.253	15.104	13.032	13.528	14.123
Part. density (10^{23}cm^{-3})	242.58	278.54	314.50	192.77	240.74	288.70	336.66	314.76	374.72	434.70
Coord. number	3.78	3.76	3.75	3.94	3.90	3.87	3.86	3.94	3.92	3.90
Crystal structure	Hex.	Hex.	Hex.	Hex.	Hex.	Hex.	Hex.	Hex.	Hex.	Hex.
Symmetry groups	$P3_1m$ IT 156	$P3_1m$ IT 156	$P3_1m$ IT 156	$P6_3/mc$ IT 186	$P6_3/mc$ IT 186	$P6_3/mc$ IT 186	$P6_3/mc$ IT 186	$P3_1m$ IT 156	$P3_1m$ IT 156	$P3_1m$ IT 156
Unit cell (atoms)	242	278	314	192	240	288	336	314	374	434
Lat. param. Å (a,c)	29.694 5.420	33.008 5.422	36.314 5.426	23.035 5.388	26.335 5.396	29.631 5.399	32.925 5.406	29.616 5.387	32.918 5.392	36.220 5.395
Average bond Å	2.005	2.005	2.004	2.012	2.011	2.010	2.009	2.013	2.012	2.011
Average angle Zn-O-Zn/O-Zn-O	108.96 110.59	108.01 110.68	109.89 110.75	109.33 189.75	109.24 109.93	109.17 110.06	109.12 110.15	109.34 109.73	109.28 109.84	109.24 109.92
Band gap eV	3.772	3.762	3.757	3.797	3.779	3.758	3.729	3.764	3.731	3.700
UC Connolly surface area Å^2	522.31	647.22	770.21	80.08	211.97	333.32	458.65	144.39	217.26	393.70
UC Pore vol. Å^3	1137.7	1688.6	2323.9	44.44	215.06	498.37	876.85	133.32	352.80	691.18
Num vib.mod.	726	834	942	576	720	864	1008	942	1122	1302
Bulk modulus	16.31	14.24	12.68	39.1	30.96	25.56	21.69	38.3	31.96	27.17

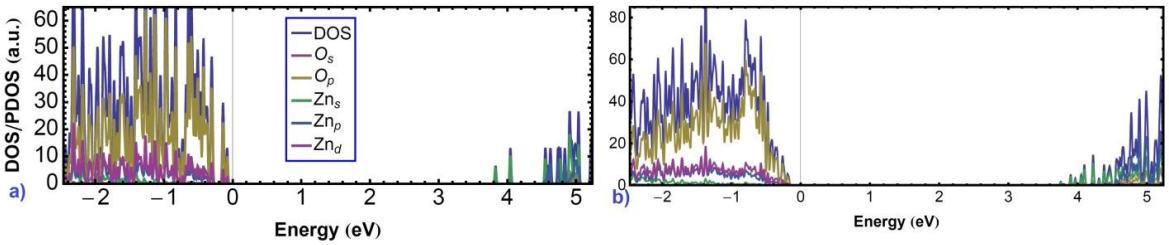

Figure 6. Projected density of states (PDOS) of SW-2 (a) and SW-3 (b). Fermi energies are set to zero.

Overall, our result confirms that the energy gap, which is an important parameter towards technological applications, is sensitive to crystal hollow thickness.

To obtain deeper insight into the electronic structure, the corresponding orbital-projected atomic density of states are given in Fig. 6. Examinations of the valence band maximum (VBM) and conduction band minimum (CBM) show that the electronic bands are made mainly by O-2*p* with some small contribution from Zn-3*d* and Zn-4*s* states, respectively. Further, O-2*p* and Zn-3*d* states are mainly distributed in the energy window of 0.2~2.0 eV below the VBM showing a strong their hybridization.

The frontier electronic orbitals, i.e. highest occupied molecular orbital (HOMO) and lowest unoccupied molecular orbital (LUMO) levels, and their charge density differences for SW-2 structure, are also plotted in Fig. 7. There orbital contribution to the VBM and CBM can clearly be seen from the HOMO and LUMO states where the VBM are localized mostly on the anions (O-sites) and the LUMO states on the cations (Zn-sites). It also evidences that the VBM receives contributions mainly from planar *py*, *px* and *dxy*, dx^2-y^2 atomic orbitals. Additionally the iso-density concentration around O atoms forming semi-torus lobes and converging towards the hollow center shows the presence of dangling bonds and surface effect (Fig. 7b), which can also be observed clearly in the charge density difference (Fig. 7c).

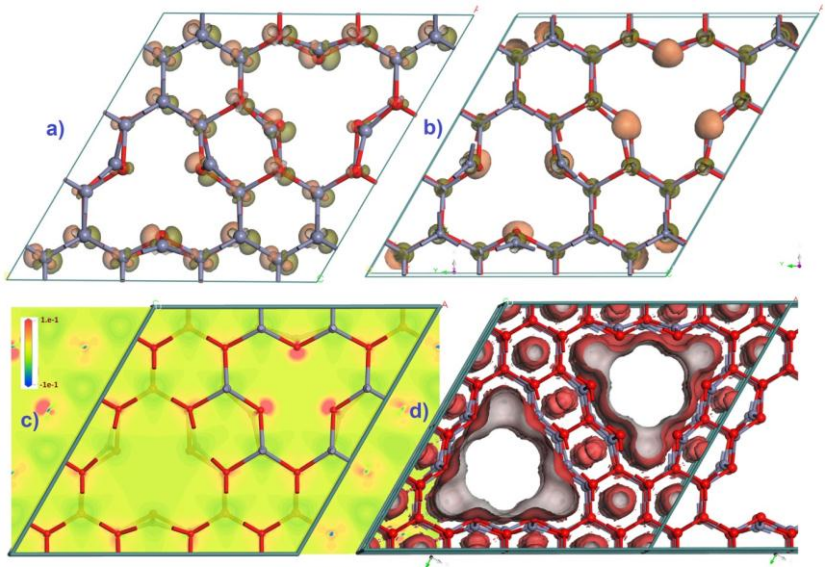

Figure 7. HOMO and LUMO states, charge density differences of SW-2 and connoly surface of SW-3.

4. Other remarks

The hexagonal wire connected by six bridges, serving as the hollow wall (see Fig 1 first structure, i.e. SW-2), shape of the structures designed in this work is a clear advantage. In particular, this suggests that a template containing aligned ultra-dense array of hexagonal nanowires may be suitable for casting these predicted hollow structures. Furthermore, we have estimated the pore volume and specific surface area (see Table 1), which reflect the porosity of their framework. Other essential structural parameters, such as the lattice contents, mass density, space group, bond statistics, are also listed in Table 1. The band structure and PDOS and the analysis show that the average coordination number for any structure is almost four (except some small dangling due to the internal hollow cage surface), i.e. each Zn (O) atom has nearly four O (Zn) neighbors forming distortional sp^3-type

hybridizations for almost all structures. Thus it may result in preserving the valuable properties of the ZnO materials, such as semiconducting, piezoelectricity and optical transparence. Generally the studied can be divided into two sub-groups differing by the symmetry group as (i) the single SW and triple wall (TW) thickness with IT number 186 ($P6_3$/mc C6V-4), i.e. same as wurtzite ZnO and (iii) double wall (DW) and four wall (4W) thickness with IT number 156 (P31m C3V-1).

As shown in Table 1, the volume per atom of ZnO hollow structures higher than the WZ, respectively, from 8.4% up to 213% larger than that of wurtzite ($11.9Å^{-3}$). Naturally, it leads to higher flexibility and compressibility (lower BM) of the new hollow phases. Therefore, these new nanoporous phases if synthesized, will be the promising candidates of mechanical meta-materials for replacing the expensive and mechanically fragile atomic or molecular selective materials [40]. Their gap-engineering and large internal surface area of the hollow channel also serve as promising solutions for efficient *solar-to-chemical* energy conversion and photoelectrochemical water splitting alternately to TiO_2 micro/nano patterned structures [41].

5. Conclusion

To date, the nanoporous *open-framework* materials have been increasingly important because of their ability to control pore's sizes and shapes, which help tailoring their physical and chemical properties for particular applications. The main interest on these nanoporous allotropes is due to their capability to interact with ions or atoms both throughout their bulk and their internal surfaces, which makes them very useful especially as catalysis or as membranes. Our theoretical studies enable the predictions of a class of ZnO crystal nanoporous structures, which exhibit the same symmetry with wurtzite ZnO but are different in hollow size and wall thickness. Our analysis on their structural, electronics and the thermodynamic properties clearly reveal that, these hollow allotropes may describe the real nanoporous and low-density crystaline materials. The important factors for practical application are their ability for gap-engineering, different pore size and thickness and the trend approaching the bulk streng-to-density with increasing the porosity. Furthermore, we believe that these nanoporous structures can be the prototype for other II-VI semiconducting materials, such as ZnS, CdSe, and CdTe.

6. Supplementary materials

See the supplementary materials for the images, complete electronic structure and detail table of characteristics as well as the coordination files.

Acknowledgements

This work was supported by Vietnam National Foundation for Science and Technology Development (NAFOSTED) under grant number 103.01-2014.25.

References

[1] A. K. Cheetham, G. Férey, and T. Loiseau, Angew. Chem. Int. Ed. 38, 3268 (1999).

[2] R. M. A. Roque-Malherbe, The Physical Chemistry of Materials: Energy and Environmental Applications.: CRC Press, 2016.

[3] P. Guo, J. Shin, A. G. Greenaway, J. G. Min, J. Su, H. J. Choi, L. Liu, P. A. Cox, S. B. Hong, P. A. Wright, and X. Zou, Nature 524, 74 (2015).
[4] R. Xu, W. Pang, J. Yu, Q. Huo, and J Chen, Chemistry of Zeolites and Related Porous Materials: Synthesis and Structure.: John Wiley & Sons, 2009.
[5] W. J. Roth, P. Nachtigall, R. E. Morris, P. S. Wheatley, V. R. Seymour, S. E. Ashbrook, P. Chlubná, L. Grajciar, M. Položij, A. Zukal, and J. Čejka, Nat. Chem. 5, 628 (2013).
[6] Y. Tian, Y. Zhang, T. Wang, H. L. Xin, H. Li, and O. Gang, Nat. Mater. 15, 654 (2016).
[7] H. Xiong, M. Y. Sfeir, and O. Gang, Nano Lett. 10, 4456 (2010).
[8] J. Bauer, A. Schroer, R. Schwaiger, and O. Kraft, Nat. Matter. 15, 438 (2016).
[9] M. Willander, Zinc Oxide Nanostructures Advance and Applications.: Pan Stanford, 2014.
[10] Z. L. Wang, J. Phys.: Condens. Matter 16, R829 (2004).
[11] Z. L. Wang and J. Song, Science 312, 242 (2006).
[12] F. Pan, C. Song, X. J. Liu, Y. C. Yang, and F. Zeng, Mater. Sci. Eng. R., Rep. 62, 1-35 (2008).
[13] V. N. Tuoc, T. D. Huan, and L. T. H. Lien, IEEE Trans. Magn. 50, 2400407 (2014).
[14] A. B. Djurišić, Ng. A. M. C., and X. Y. Chen, Prog. Quant. Electron. 34, 191 (2010).
[15] A. Kołodziejczak-Radzimska and T. Jesionowski, Materials 7, 2833 (2014).
[16] Y. Yong, Song B., and He P., J. Phys. Chem. C 115, 6455 (2011).
[17] I. Demiroglu, S. Tosoni, F. Illasa, and S. T. Bromley, Nanoscale 6, 1181 (2014).
[18] Z. Liu, X. Wang, J. Cai, G. Liu, P. Zhou, K. Wang, and H. Zhu, J. Phys. Chem. C 117, 17633 (2013).
[19] S. M. Woodley and R. Catlow, Nat. Mater. 7, 937 (2008).
[20] A. A. Sokol, M. R. Farrow, J. Buckeridge, A. J. Logsdail, C. R. A. Catlow, D. O. Scanlonab, and S. M. Woodley, Phys. Chem. Chem. Phys. 16, 21098 (2014).
[21] V.N. Tuoc, T.D. Huan, N.T. Thao and L.M. Tuan, Journal of Applied Physics 120, 142195 (2016).
[22] Y. Yong, X. Li, X. Hao, J. Cao, and T. Li, RSC Adv. 4, 37333 (2014).
[23] M. Elstner, D. Porezag, G. Jungnickel, J. Elsner, M. Haugk, Th. Frauenheim, S. Suhai, and G. Seifert, Phys. Rev. B 58, 7260 (1998).
[24] C. Kohler, G. Seifert, and T. Frauenheim, Chem. Phys. 309, 23 (2005).
[25] B. Aradi, B. Hourahine, and Th. Th. Frauenheim, J. Phys. Chem. A 111, 5678 (2007).
[26] DFTB+. [Online]. http://www.dftb-plus.info/
[27] N. H. Moreira, G. Dolgonos, B. Aradi, A. L. da Rosa, and Th. Frauenheim, J. Chem. Theory Comput. 5, 605 (2009).
[28] V. N. Tuoc, Comput. Mater. Sci. 49, S161 (2010).
[29] G. Kresse and J. Furthmüller, Comput. Mater. Sci. 6, 15 (1996).
[30] G Kresse and J. J. Furthmüller, Phys. Rev. B 54, 11169 (1996).
[31] J. P. Perdew, K. Burke, and M. Ernzerhof, Phys. Rev. Lett. 77, 3865 (1996).
[32] J. P. Perdew, A. Ruzsinszky, G. I. Csonka, O. A. Vydrov, G. E. Scuseria, L. A. Constantin, X. Zhou, and K. Burke, Phys. Rev. Lett. 100, 136406 (2008).
[33] J. Heyd, G. E. Scuseria, and M. M. Ernzerhof, J. Chem. Phys. 124, 219906 (2006).
[34] C.-L. Fu and K.-M. Ho, Phys. Rev. B 28, 5480 (1983).
[35] T. D. Huan, arXiv preprint , arXiv:1506.09189 (2015).
[36] L. Sponza, J. Goniakowski, and C. Noguera, Phys. Rev. B 91, 075126 (2015).
[37] V. N. Tuoc, T. D. Huan, and L. T. H. Lien, Phys. Status Solidi B 249, 1241 (2012).
[38] M. A. Zwijnenburg, F. Illas, and S. Bromley, Phys. Rev. Lett. 104, 175503 (2010).
[39] M. A. Zwijnenburg and S. Bromley, J. Mater. Chem. 21, 15255 (2011).
[40] J. H. Lee, J. P. Singer, and E. L. Thomas, Adv. Mater. 24, 4782 (2012).
[41] Z. Xu, M. Yin, J. Sun, G. Ding, L. Lu, P. Chang, X. Chen, and D. Li, Nanotechnology 27, 115401 (2016).